GA–A26758

OEDGE MODELING OF THE DIII-D DOUBLE NULL $^{13}CH_4$ PUFFING EXPERIMENT

by

J.D. ELDER, W.R. WAMPLER, A.G. McLEAN, P.C. STANGEBY,
S.L. ALLEN, B.D. BRAY, N.H. BROOKS, A.W. LEONARD,
E.A. UNTERBERG, and J.G. WATKINS

JULY 2010

GENERAL ATOMICS

DISCLAIMER

GA–A26758

OEDGE MODELING OF THE DIII-D DOUBLE NULL $^{13}CH_4$ PUFFING EXPERIMENT

by

J.D. ELDER*, W.R. WAMPLER†, A.G. McLEAN‡, P.C. STANGEBY*, S.L. ALLEN¶, B.D. BRAY, N.H. BROOKS, A.W. LEONARD, E.A. UNTERBERG‡, and J.G. WATKINS†

This is a preprint of a paper to be presented at the Nineteenth International Conference on Plasma Surface Interactions, May 24-28, 2010, in San Diego, California, and to be published in *J. Nucl. Mater.*

*University of Toronto Institute for Aerospace Studies,Toronto, Canada.
†Sandia National Laboratories, Albuquerque, New Mexico.
‡Oak Ridge National Laboratory, Oak Ridge, Tennessee.
¶Lawrence Livermore National Laboratory, Livermore, California.

Work supported in part by
the U.S. Department of Energy
under DE-AC04-94AL85000, DE-AC05-00OR22725,
DE-AC52-07NA27344, and DE-FC02-04ER54698

GENERAL ATOMICS PROJECT 30200
JULY 2010

ABSTRACT

ITER plans to use a single null configuration with a secondary upper X-point just outside the upper target. The plasma interaction at the ITER secondary outer strike point was simulated on DIII-D using an unbalanced double null ELMy H-mode configuration. The measured plasma conditions in the outer secondary divertor closely duplicated those projected for ITER. $^{13}CH_4$ was injected into the secondary outer divertor to simulate sputtering there. The majority of the ^{13}C found was in the secondary outer divertor. This material migration pattern is radically different than that observed for main wall $^{13}CH_4$ injections into single null configurations where the deposition is primarily at the inner divertor. The implications for tritium codeposition resulting from sputtering at the secondary divertor in ITER are significant since release of tritium from Be co-deposits at the main wall bake temperature for ITER, 240°C, is incomplete. The principal features of the measured ^{13}C deposition pattern have been replicated by the OEDGE interpretive code.

I. INTRODUCTION

Co-deposition processes do not saturate and could result in an unacceptable buildup of tritium inventory in next-generation fusion devices. In ITER, the secondary outer divertor region is a particular concern since it can only be baked to 240°C, whereas the main divertor can be baked to 350°C. Release of T from Be co-deposits is only partial at 240°C [1], as is recovery from C co-deposits using oxygen-baking [2]. The objective of this experiment on DIII-D was to assess the migration pattern of impurities produced near the secondary strike point and assess the significance of the results in the context of ITER requirements.

The injection of $^{13}CH_4$ into the edge of tokamaks has been shown on TEXTOR [3], JET [4] and DIII-D [5,6], among others, to provide valuable opportunities for diagnosis of edge transport and carbon behavior. In the current experiment, $^{13}CH_4$ methane was puffed in a toroidally symmetric way into the secondary outer strike point region of a set of identical unbalanced double null discharges. The $^{13}CH_4$ methane was released through the lower outer baffle and entered the plasma region under the shelf at the bottom of the torus directly into the secondary outer divertor (Fig. 1). Puffing continued for a period of 2 s in each of 18 consecutive identical 1.2 MA ELMy H-mode discharges with 6.5 MW of neutral beam heating. Nominal secondary strike point plasma conditions of $n_e = 1 \times 10^{19}$ m^{-3} and $T_e = 10$ eV were achieved during the experiment, comparable to those projected for the secondary separatrix in ITER, i.e. 0.5-1.5$\times 10^{19}$ m^{-3} and $T_e = 10$-20 eV [7]. Tiles from around the torus were removed immediately after the experiment and the ^{13}C surface content was measured using nuclear reaction analysis (NRA) [8,9].

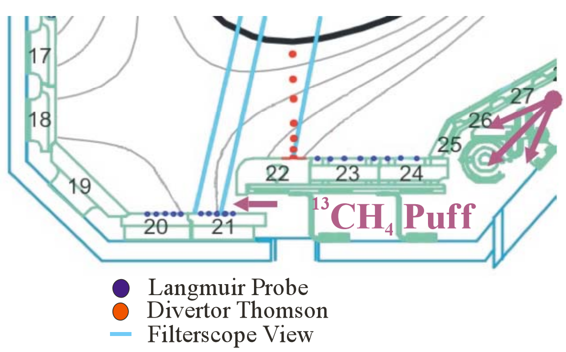

Fig. 1. Magnetic configuration and diagnostic locations.

This paper investigates the transport and deposition of carbon originating from the ^{13}C methane puffing in this experiment. The NRA measurements of ^{13}C by W.R. Wampler are first reported and then the model results examined. The onion-skin model/EIRENE/DIVIMP edge (OEDGE) interpretative modeling code [10] is used to model the release, breakup, transport and deposition of the ^{13}C. OEDGE has been successfully applied to interpretive modeling of the previous $^{13}CH_4$ experiments on DIII-D [11-14].

II. ^{13}C DEPOSITION RESULTS

The ^{13}C concentration on the surface of the tiles was measured by NRA (Fig. 2). The greatest concentration was found in the secondary outer divertor near the pumping duct with smaller deposits on top of the shelf and at the upper inner primary target. No significant deposition was found at the upper outer primary target, the secondary inner target or on main vessel wall surfaces. NRA measurements of the deposition accounted for 48% of the injected amount of ^{13}C. Of the total puffed ^{13}C, 28% was deposited on the tile immediately at the entrance to the puffing duct, 6% was deposited on the nose of the shelf tile, 12% on the upper surface of the shelf and an additional 2% at the inner primary target. These numbers include deposition in the tile gaps where these data are available. Deposition of ^{13}C down the tile gap on tile 21 was very small with an exponential decay length less than 1 mm. The disposition of the remaining ^{13}C is unknown at this time.

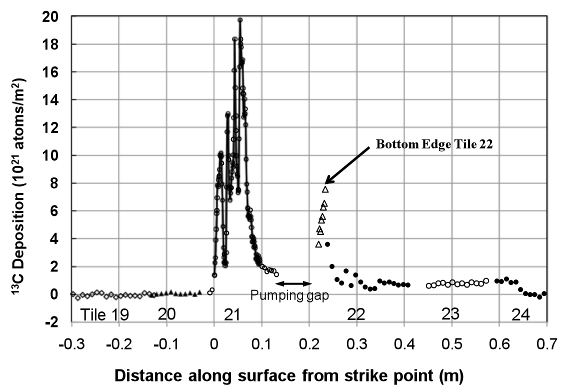

Fig. 2. Measured ^{13}C deposition on the floor tiles.

III. OEDGE MODELING RESULTS

The first step in the OEDGE analysis was to use experimental data and “onion-skin” modeling (OSM) to infer a solution for the background plasma by empirical reconstruction [11,15]. Empirical plasma reconstruction utilizes experimental data and 1D onion-skin models along each flux tube of the modeling grid to generate background plasma solutions which are then used for calculating the transport and deposition of the ^{13}C in the rest of the study.

The $^{13}CH_4$ gas is introduced in the modeling as neutral molecules through the lower pumping duct. Each $^{13}CH_4$ molecule and resulting ^{13}C particle (atom or ion) is followed using DIVIMP through a series of molecular breakup processes, atomic processes, and surface interaction processes until the ^{13}C leaves the simulation by depositing on a surface. The resulting deposition is compared to the experimental values.

Hydrocarbon sticking coefficients from Jacob [16] were used in the simulations. Carbon neutrals and ions were assumed to stick when striking a surface. Code results are calibrated to the absolute amount of $^{13}CH_4$ puffed and are thus directly comparable to the experimental results for both distribution and magnitude. The simulations reported here only examined the deposition of ^{13}C local to the secondary outer divertor.

There are three diagnostic measurements used in this analysis: Langmuir probe measurements of target J_{sat} and T_e, divertor Thomson measurements of n_e and T_e just above the shelf and filterscope measurements of D_α, CII-515 nm and CIII-465 nm emissions for lines of sight in or near the secondary outer divertor (Fig. 1). The Langmuir probe data are used as input to the OSM which then iterates with EIRENE to include the effect of recycling hydrogen on the background plasma solution.

Examination of the between ELM base line spectroscopic measurements (Fig. 3) show an increase in both carbon and hydrogen emissions as a result of the puffing. The puff was started at 2500 ms. An initial rise in emissions is seen after 100 to 200 ms while it takes roughly 500 to 600 ms for the effect of the puff to be fully realized. In addition, the level of emissions is gradually increasing during the shot indicating that the plasma is not in a complete steady state; however, the behavior of consecutive discharges in the set is very similar. CIII-465 nm emissions on chords viewing the secondary outer divertor rise by 20 to 30%. An increase of D_α of roughly 10% is seen on the chord viewing the plasma closest to the baffle. The D_α emission near the secondary divertor strike point appears unaffected by the puff (not shown).

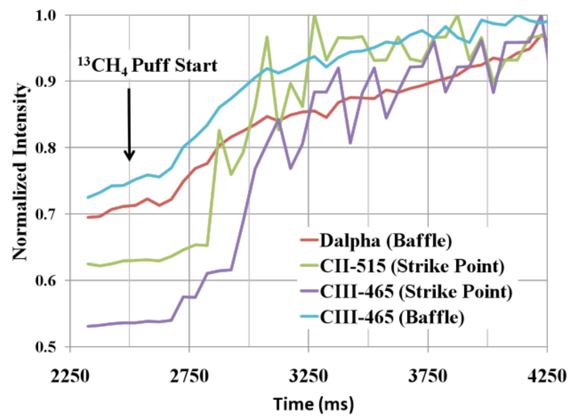

Fig. 3. Normalized filterscope intensities over time.

Examination of the between ELM Langmuir probe J_{sat} measurements during the discharge show that the J_{sat} at the secondary strike point is unaffected by the puff while the probes nearest the puff entry location show a reduction of ~40% (Fig. 4). The time required for this reduction is comparable to that seen in the filterscope measurements. The Langmuir probes show no measurable change in target T_e in response to the puffing. The lack of change in T_e combined with a ~40% drop in corresponding target J_{sat} indicates that the local plasma density, at least downstream from the puff, may also have dropped. This could locally increase the mean free path for $^{13}CH_4$ fragment breakup allowing for greater penetration of the fragments and an increased likelihood for particle escape from the divertor. These effects are included in the simulations.

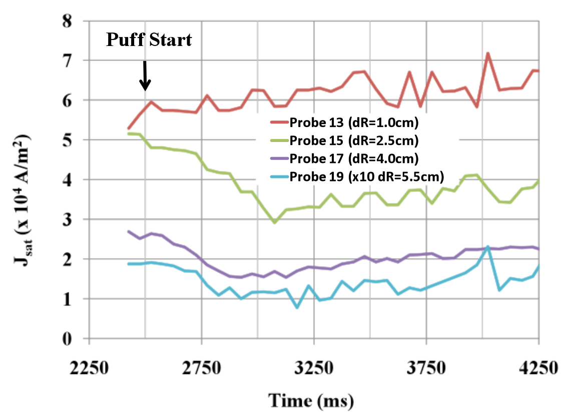

Fig. 4. Langmuir probe measurements of secondary divertor between-ELM J_{sat} over time.

The OSM solution and ^{13}C transport is based on the between ELM plasma conditions since those represent the more prevalent conditions in the divertor. However, the greater plasma intensity associated with ELMs could have a significant effect on erosion and deposition. Multiple erosion/deposition steps could be a factor in the ^{13}C migration in the divertor. However, the substantial ^{13}C deposits seen experimentally even near the strike point would tend to indicate that erosion by ELMs did not play a large role in this experiment. The input density and temperature used in the OSM are shown in Fig. 5.

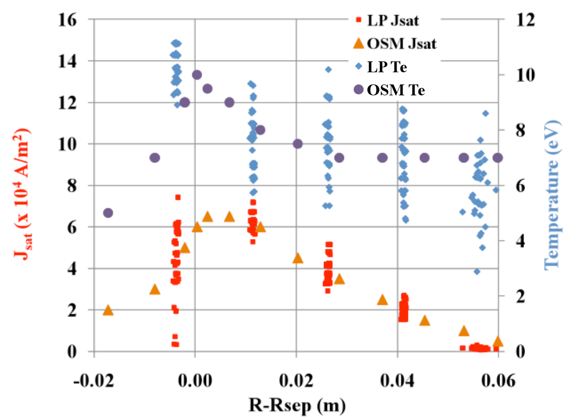

Fig. 5. Langmuir probe J_{sat} and T_e across the target with OEDGE input data.

As can be seen in the filterscope measurements the methane puffing causes some change in the divertor D_α emission. It is possible that this change is due to the changes in the local plasma conditions. However, the methane gas itself delivers a non-negligible amount of hydrogen to the plasma. The maximum total ^{13}C influx into the plasma is 2.55×10^{22} atoms of ^{13}C over 18 discharges with 2 s of puffing plus a decay time in each. This yields a maximum hydrogen influx of about 3×10^{21} H/s compared to the total secondary outer divertor target flux of roughly 8×10^{21} H/s. This could have a non-negligible effect on the plasma mass balance in the secondary outer divertor. This possibility is explored by adding an H_2 gas puff from the lower duct in the EIRENE simulations.

Results from two simulation cases are presented in Fig. 6. In the first case, only the hydrogen recycling at the target has been included in the OSM calculations of the plasma solution. This results in stronger local deposition at the edge of the plasma in the outer secondary divertor. In the second case, the addition of a hydrogen puff from the duct of 9.4×10^{20} H/s increases the simulated local hydrogen D_α emission on the view chord looking just below the baffle by about 10%. This increase is comparable to the increase seen experimentally. The puff affects the net parallel particle flux on the flux tubes closest to the pump duct opening. This leads to stronger frictional transport of material along the secondary SOL away from the target reducing local deposition at the edge of the plasma and transporting some ^{13}C out of the divertor.

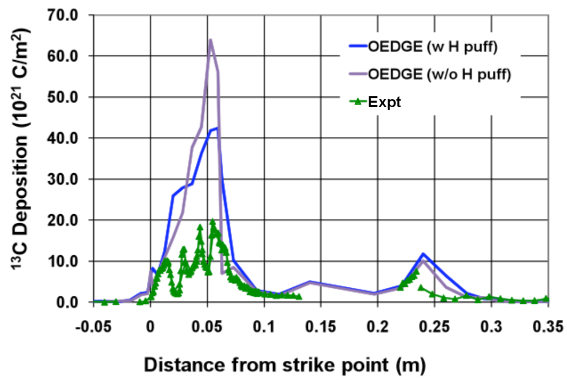

Fig. 6. OEDGE calculated ^{13}C deposition with the experimental measurements. Shown are cases with and without an additional H puff.

Figure 6 shows the deposition on tiles 21 and 22 comparing the experimental measurements to the simulation results for these two cases. The long flat deposition region above the shelf on tiles 23 and 24 (not shown here) is not reproduced. The deposition in this region may be due to methane leakage from the lower outer baffle plenum into the area above the shelf through tile gaps. It is also possible that radial transport near the outer midplane is not diffusive which could distribute the ^{13}C escaping from the divertor more uniformly across the shelf.

IV. DISCUSSION

The measured deposition on tile 21 contains dips in the profile that are not reproduced by the simulations (Figs. 6,7). Surface profilometry was used to look for structural differences in the surface at these regions but no significant differences in surface structure were found. The history of strike point locations and particle fluxes for the outer divertor were also mapped but no correlation between the deposition pattern and the historical plasma data was found. The possibility of erosion by ELMs or arcing is still being examined.

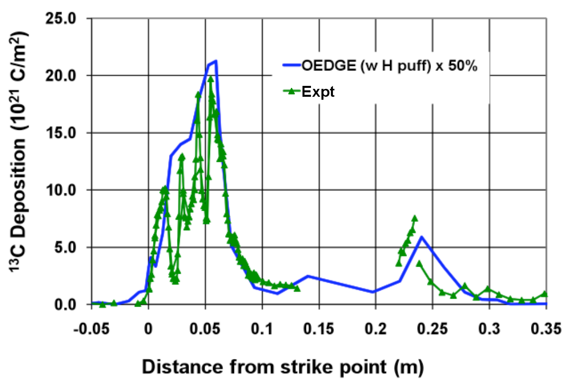

Fig. 7. OEDGE calculated ^{13}C deposition for the case with an additional H puff affecting the background plasma calculations. (Scaled by 50%).

It seems likely that the $^{13}CH_4$ puff had a moderate effect on the local plasma conditions, modifying both carbon and hydrogen emissions as well as the target ion fluxes and the deuterium mass balance. Simulations indicate that a hydrogen influx through the pumping duct consistent with the spectroscopic measurements and the total available hydrogen from the methane puff would drive a parallel ion plasma flow toward the outer mid-plane along the magnetic field on the outermost flux tubes due to the increased ion source on these flux tubes. A flow of this type reduces the target deposition and increases the carbon that is available to deposit on the shelf and elsewhere in the vessel. Code results were found to be sensitive to the specific target conditions used for the outer most flux tubes in the divertor.

In any case, the majority of the ^{13}C found experimentally remains on the target in the secondary outer divertor region. It is important to note that such a material migration pattern is radically different than has been observed in single null studies on DIII-D [5,6], JET [4] and others, where injection into the crown of the plasma, or other wall locations, resulted in the main ^{13}C deposition occurring in the inner (primary) divertor.

The ^{13}C experimental measurements indicated deposition only near the methane puff region and at the inner primary target. This may be an indication of SOL flows toward the inner divertor in the primary SOL even in this double null configuration since no deposition was found at the upper outer primary target.

Leaks in the baffle volume to both the main vessel and vessel structure through tile gaps and other openings, the amount of residual gas in the baffle volume, and the experimental uncertainty in the calculation of the total ^{13}C entering the system, all contribute to the likelihood that the amount of ^{13}C entering the secondary outer divertor plasma during the experiment was less than the maximum value of 2.55×10^{22}. The estimate of ^{13}C entering the system is based on calibrated pressure transducer measurements located at the valve in the ^{13}C gas source supply line, i.e. remote from the plenum. A 50% discrepancy in total ^{13}C entering through the pumping duct leads to an essentially perfect match between simulation and experimental measurements (Fig. 7).

The OEDGE code simulations are able to reproduce the major features of the experimental ^{13}C deposition. The code reports deposition at the target, on the leading edge of the shelf and some ^{13}C crossing the secondary separatrix. The code does not reproduce the broad flat deposition seen on the top of the shelf on tiles 23 and 24. A broad flat deposition profile could be obtained by fast radial ion transport. However, no ^{13}C deposition is measured on the outer wall which might be expected if there were enhanced radial ion transport. The flat shelf deposition may be due to $^{13}CH_4$ leaking from the plenum into the main vessel through tile gaps. ^{13}C deposition in the pumping duct itself is due to sticking of neutral carbon and neutral hydrocarbon fragments resulting from the break up of the puffed methane at the edge of the plasma.

V. CONCLUSIONS

ITER plans to use a single null configuration with a secondary upper X-point just outside the upper target. The plasma interaction at the ITER secondary outer strike point was simulated on DIII-D using an unbalanced double null ELMy H-mode configuration. The measured plasma conditions in the outer secondary divertor closely duplicated those projected for ITER. $^{13}CH_4$ was injected into the secondary outer divertor to simulate sputtering of beryllium there. At the ITER reference plasma conditions of $n_e = 10^{19}$ m^{-3} and $T_e = 10$ eV, the ionization mean free path of carbon (0.5 eV) from methane breakup is similar to that for physically sputtered Be (3 eV). Thus, the deposition pattern found in this experiment for ^{13}C may be similar to that for beryllium.

The majority of the ^{13}C found was in the secondary outer divertor. This material migration pattern is radically different than has been observed for main wall injections into single null configurations. The implications for tritium codeposition resulting from sputtering at the secondary divertor in ITER are significant since release of tritium from Be co-deposits at the main wall bake temperature for ITER, 240°C, is incomplete.

The principal features of the measured ^{13}C deposition pattern have been replicated by the OEDGE interpretive code, supporting the likelihood that this material migration pattern can be expected to occur in ITER. Indeed, because of the larger physical scale of ITER, the plasma in the secondary divertor will be still more opaque to the incoming impurity neutrals, and the deposition is likely to be still more localized, than occurred in DIII-D.

REFERENCES

[1] R.P. Doerner, *et al*., Nucl. Fusion **49**, 035002 (2009).

[2] J.W. Davis and A.A. Haasz, J. Nucl. Mater. **390-391**, 532 (2009).

[3] P. Wienhold, *et al*., J. Nucl. Mater. **290-293**, 362 (2001).

[4] J. Likonen, *et al*., Fusion Engin. Design **66-68**, 219 (2003).

[5] S.L. Allen, *et al*., J. Nucl. Mater. **337-339**, 30 (2005).

[6] M. Groth, *et al*., Phys. Plasmas **14**, 056120 (2007).

[7] M. Shimada, *et al*., Heat and Nuclear Load Specifications for ITER.

[8] W.R. Wampler, *et al*., J. Nucl. Mater. **363-365**, 72 (2007).

[9] W.R. Wampler, *et al*., J. Nucl. Mater. **337-339**, 134 (2005).

[10] P.C. Stangeby, *et al*., J. Nucl. Mater. **313-316**, 883 (2003).

[11] J.D. Elder, *et al*., J. Nucl. Mater. **337-339**, 79 (2005).

[12] J.D. Elder, *et al*., J. Nucl. Mater. **363–365**, 140 (2007).

[13] A.G. McLean, *et al*., J. Nucl. Mater. **337-339**, 124 (2005).

[14] J.D. Elder, *et al*., J. Nucl. Mater. **390–391**, 376 (2009).

[15] S. Lisgo, *et al*., J. Nucl. Mater. **337-339**, 256 (2005).

[16] W. Jacob, J. Nucl. Mater. **337-339**, 839 (2005).

ACKNOWLEDGMENT

The authors would like to acknowledge the support of a Collaborative Research Opportunities Grant from the Natural Sciences and Engineering Research Council of Canada and the U.S. Department of Energy. This work supported in part by the U.S. Department of Energy under DE-AC04-94AL85000, DE-AC05-00OR22725, DE-AC52-07NA27344, and DE-FC02-04ER54698.